Real space analysis of the nonlocal optical response of PPV oligomers

Thomas Wagersreiter and Shaul Mukamel
Department of Chemistry, University of Rochester, Rochester, New York 14627

(Received 4 October 1995; accepted 5 February 1996)

We investigate the linear optical polarizabilities of poly(p-phenylene vinylene) oligomers using the time dependent Hartree Fock procedure. Our analysis is based on the computation of a nonlocal response function, which describes the effects of an interaction with the electromagnetic field at one carbon atom on the distribution of charges at other atoms. This provides physical insight into intramolecular charge dynamics and the anisotropic tensorial properties of the linear polarizabilities. The results are analyzed using the coupled electronic oscillator (CEO) representation, which allows the assignment of absorption peaks to distinct transitions between Hartree Fock orbitals. The size dependence of the linear absorption shows that at 10 repeat units the optical gap has almost converged to its infinite size value, and the oscillator strength of the lowest absorption line scales linearly with size. This implies that the sizes studied exceed the exciton coherence size and the resulting spectra should mimic the infinite size limit. [S0021-9606(96)50418-1]

I. INTRODUCTION

π conjugated polymers have become the subject of intense studies, as they can be used in a variety of electro-optical applications, including conducting polymers (after doping) and light emitting diodes. The particular interest in poly(p-phenylene vinylene) (PPV) and its derivatives, stemming from their electroluminescence and unusually large second and third order response, has greatly increased since its preparation in form of high quality thin films.[1–3]

Experimental investigations include Raman, infrared, and UV/visible spectra,[1,4–6] photoinduced absorption,[7] and site selective fluorescence studies.[8] Anisotropy in the linear response and the third order susceptibility have been measured and a model of the lowest-energy electronic transition has been proposed.[1,9,10] Resonance Raman spectroscopy has been used to characterize polarons and bipolarons.[5] In order to clarify the nature of the various excitations in PPV, a variety of time resolved measurements were carried out. Picosecond photoinduced absorption[11] was used to identify polaron pairs and spatially indirect excitons in PPV films. Time resolved fluorescence measurements could be successfully interpreted in terms of the Förster dynamics of excitons in a system with inhomogeneously broadened density of states.[12]

Early theoretical investigations focused on the calculation of band structures. Single chain, 1D band structures have been computed.[13,14] The first 3D band structure was calculated using a local density functional method,[15] in order to investigate the effects of interchain coupling. Other methods employed for the calculation of IR to UV spectra include the theory of the effective conjugation coordinate (EEC),[6] semiempirical molecular orbital (MO) calculations at the intermediate neglect of differential overlap (INDO) and Pariser-Parr-Pople (PPP) levels, and valence effective Hamiltonian (VEH) techniques.[16,17] Since such methods are computationally costly, they cannot be applied to large systems, and a number of simpler models have been devised. Rice and Gartstein proposed a model for the photoexcitations of PPV polymers, based on four states in each phenylene monomer, which captures the essential photophysics in these systems.[18] Su-Schrieffer-Heeger (SSH) Hamiltonians which neglect electron-electron correlations, but include electron-phonon coupling are used to investigate vibrational properties of PPV.[14]

In this work, we analyze the optical spectra of PPV oligomers with up to 10 repeat units by means of nonlocal electronic response functions. The approach is based on the reduced single electron density matrix obtained by solving the time dependent Hartree Fock (TDHF) equations for the PPP Hamiltonian.[19] This method provides direct information on charge distribution and electronic coherences within the molecules. Using the density matrix we calculate a nonlocal response function $\tilde{\alpha}_{nm}$, which relates the induced charges to the driving field, thereby revealing the mechanism of the optical response. The full polarization tensor can then be easily calculated without invoking the dipole approximation. Nonlocal response functions represent a convenient approach to study charge dynamics.[21–24] Hunt and coworkers investigated force-balance between molecules, response of molecules to (infinitesimal) shifts of their nuclear coordinates, and electric field shielding tensors.[20] Chernyak, Jenkins and Mukamel studied the nonlocal optical response of molecular aggregates[22,23] and conjugated molecules.[24]

In order to interpret the absorption spectra we make use of the coupled electronic oscillator (CEO) representation[19,25] and compute the oscillators relevant for the linear response. By depicting them in the Hartree Fock Molecular Orbital (HFMO) representation we identify the optical transitions between the relevant HFMOs.

In Sec. II we provide a brief review of the PPP Hamiltonian and the method used for solving the TDHF equations.[19] We also outline how it may be used for the computation of the nonlocal response tensor. We then apply this method to PPV oligomers and present the linear polarizability in Sec. III. Thereafter we analyze the optical re-

 0021-9606/96/104(18)/7086/13/$10.00

sponse using the CEO representation in Sec. IV, and summarize our results in Sec. V.

II. THE PPP MODEL AND THE TDHF EQUATIONS

In order to describe the optical properties of conjugated molecules such as PPV oligomers we adopt the PPP Hamiltonian for π-electrons:[19,26]

$$\hat{H}=\sum_{n,m,\sigma} t_{nm}\hat{\rho}^{\sigma}_{nm}+\sum_{n}\overline{U}\hat{\rho}^{\uparrow}_{nn}\hat{\rho}^{\downarrow}_{nn}+\frac{1}{2}\sum_{n,m,\sigma,\sigma'}^{n\neq m} U_{nm}\hat{\rho}^{\sigma}_{nn}\hat{\rho}^{\sigma'}_{mm}+\hat{H}_{\rm int}, \tag{1}$$

where we have neglected electron – phonon coupling. The one electron density operator $\hat{\rho}^{\sigma}_{nm}$ is defined in terms of creation and annihilation operators $\hat{c}^{\dagger}_{n,\sigma}$, $\hat{c}_{n,\sigma}$ for an electron with spin σ at site n:

$$\hat{\rho}^{\sigma}_{nm}=\hat{c}^{\dagger}_{n,\sigma}\hat{c}_{m,\sigma}. \tag{2}$$

The first term in the Hamiltonian Eq. (1) is the Hückel Hamiltonian. Its diagonal matrix elements t_{nn} are the Coulomb integrals at site n, and off-diagonal elements t_{nm} represent electron hopping between sites n and m:

$$t_{nm}=\delta_{nm}\sum_{l} U_{nl}+(1-\delta_{nm})[\overline{\beta}-\beta'(r_{nm}-d)]. \tag{3}$$

Here $r_{nm}=|\mathbf{r}_n-\mathbf{r}_m|$ with the sites $\mathbf{r}_i, i=1,\ldots,N$, and d is the average bond-length. We have chosen the same parameters used for polyenes: $\beta=-2.4$ eV, $\beta'=-3.5$ eV. The second and third terms in the Hamiltonian describe electron-electron Coulomb interactions, where $U=7.42$ eV denotes the on-site (Hubbard) repulsion, and the repulsive interaction between sites n and m is given by Ohnos' formula

$$U_{nm}=\frac{\overline{U}}{\sqrt{1+(r_{nm}/a_0)^2}}, \tag{4}$$

with $a_0=1.2935$ Å.

In order to interpret electronic dynamics using nonlocal response functions we consider a spatially inhomogeneous electric field $\mathbf{E}(\mathbf{r},t)$. Using the multipolar Hamiltonian, the interaction with the radiation field is then given by[27]

$$\hat{H}_{\rm int}(t)=-\int d\mathbf{r}\ \mathbf{E}(\mathbf{r},t)\cdot\hat{\mathbf{P}}(\mathbf{r}), \tag{5}$$

where the polarization operator is[27]

$$\hat{\mathbf{P}}(\mathbf{r})=\sum_{\alpha} q_{\alpha}(\hat{\mathbf{r}}_{\alpha}-\mathbf{R})\int_0^1 d\lambda\,\delta(\mathbf{r}-\mathbf{R}-\lambda(\hat{\mathbf{r}}_{\alpha}-\mathbf{R})), \tag{6}$$

and α runs over all charges in the system. This operator is defined with respect to an arbitrary reference point $\mathbf{R}$, but its transverse part $\mathbf{P}^{\perp}$ is independent of $\mathbf{R}$. Upon expansion in the π–electron basis set we obtain

$$\hat{\mathbf{P}}(\mathbf{r})=\sum_{n\sigma}\hat{c}^{\dagger}_{n,\sigma}\hat{c}_{n,\sigma}\langle\psi_{n\sigma}|\hat{\mathbf{P}}(\mathbf{r})|\psi_{n\sigma}\rangle=\sum_{n\sigma}\hat{\rho}^{\sigma}_{nn}\vec{\mathscr{P}}_{n\sigma}(\mathbf{r}). \tag{7}$$

Here we have neglected the off-diagonal matrix elements of $\hat{\mathbf{P}}$. This may be rationalized by the negligible overlap of the basis functions ψ_n due to their localized nature.[28] The expansion coefficient $\vec{\mathscr{P}}_{n\sigma}(\mathbf{r})$ denotes the polarization density of the ψ_n orbital. Hence the matter-field interaction can be recast as

$$\hat{H}_{\rm int}(t)=\sum_{n\sigma}\hat{\rho}^{\sigma}_{nn}V_{n\sigma}(t), \tag{8}$$

where $V_{n\sigma}(t)$ is defined as

$$V_{n\sigma}(t)=\int d\mathbf{r}\,\vec{\mathscr{P}}_{n\sigma}(\mathbf{r})\cdot\mathbf{E}(\mathbf{r},t). \tag{9}$$

Assuming that the electronic wave function $|\Psi(t)\rangle$ can be expressed as a single Slater determinant at all times, the density-matrix elements

$$\rho^{\sigma}_{nm}(t)=\langle\Psi(t)|\hat{\rho}^{\sigma}_{nm}|\Psi(t)\rangle, \tag{10}$$

obey the TDHF equations[19]

$$i\hbar\frac{d}{dt}\rho^{\sigma}_{nm}(t)=([h^{\sigma}(t)+f^{\sigma}(t),\rho^{\sigma}(t)])_{nm}, \tag{11}$$

with

$$h^{\sigma}_{nm}(t)=t_{nm}+\delta_{nm}\sum_{l,\sigma'}U_{nl}\rho^{\sigma'}_{ll}(t)-U_{nm}\rho^{\sigma'}_{nm}(t), \tag{12}$$

and

$$f^{\sigma}_{nm}(t)=\delta_{nm}V_{n\sigma}(t). \tag{13}$$

Working with the density matrix has the advantage of dealing with physically relevant quantities (charges ρ_{nn} and electronic coherences ρ_{nm}) instead of wavefunctions. The application of this approach to multi-electron systems was extensively discussed by McWeeny.[29] Eq. (11) is a nonlinear system of differential equations that will be solved by a power series expansion in the electric field $\mathbf{E}$. To that end we define

$$\rho(t)=\overline{\rho}+\delta\rho^{(1)}(t)+\delta\rho^{(NL)}(t). \tag{14}$$

Hereafter we shall drop the spin index, restricting the calculation to spin symmetric (singlet) excitations. $\overline{\rho}$ is the reduced one-electron ground state density matrix. Its diagonal elements $\overline{\rho_{nn}}$ represent the static charge on site n, and its off-diagonal elements $\overline{\rho_{nm}}$ measure the chemical bond strength between sites n and m (bond-order). The induced density matrix is split into a term $\delta\rho^{(1)}(t)$, which is linear in the driving field, and higher order terms $\delta\rho^{(NL)}(t)$. Substituting Eq. (14) into the TDHF Eq. (11), and collecting terms to first order in the electric field leads to

$$0=[\overline{h},\overline{\rho}], \tag{15}$$

$$i\hbar\frac{d}{dt}\delta\rho^{(1)}_{nm}(t)=\sum_{rs}\mathscr{L}_{nm,rs}\delta\rho^{(1)}_{rs}(t)+A_{nm}(t), \tag{16}$$

with

$$\overline{h}_{nm}=t_{nm}+2\delta_{nm}\sum_l U_{nl}\overline{\rho}_{ll}-U_{nm}\overline{\rho}_{nm}, \tag{17}$$

$$\mathscr{L}_{nm,rs}=\delta_{ms}\overline{h}_{nr}-\delta_{nr}\overline{h}_{ms}+2\delta_{rs}(U_{ns}-U_{ms})\overline{\rho}_{nm} - \delta_{nr}U_{ns}\overline{\rho}_{ms}+\delta_{ms}U_{mr}\overline{\rho}_{nr}, \tag{18}$$

$$A_{nm}=\overline{\rho}_{nm}(V_n-V_m). \tag{19}$$

The self-consistent solution of Eq. (15)[19] yields the ground state density matrix, together with the Hartree Fock molecular orbitals c_{nm} in the form

$$\overline{\rho}_{mn}=\sum_{l=1}^{N_{\rm occ}} c_{m,l}c_{nl}, \tag{20}$$

where the sum is carried out over all occupied orbitals l. We are interested in the half filled band case, where $N_{\rm occ}=N/2$. Eq. (16) can be readily solved by a Fourier transform resulting in

$$\delta\tilde{\rho}^{(1)}_{nn}(\omega)=\sum_r \tilde{\alpha}_{nr}(\omega)V_r(\omega). \tag{21}$$

Here we have defined a nonlocal response function

$$\tilde{\alpha}_{nm}(\omega)=\sum_l (\mathscr{G}_{nn,ml}(\omega)-\mathscr{G}_{nn,lm}(\omega))\overline{\rho}_{lm}, \tag{22}$$

where

$$\mathscr{G}(\omega)=[\hbar\omega-\mathscr{L}(\omega)]^{-1}, \tag{23}$$

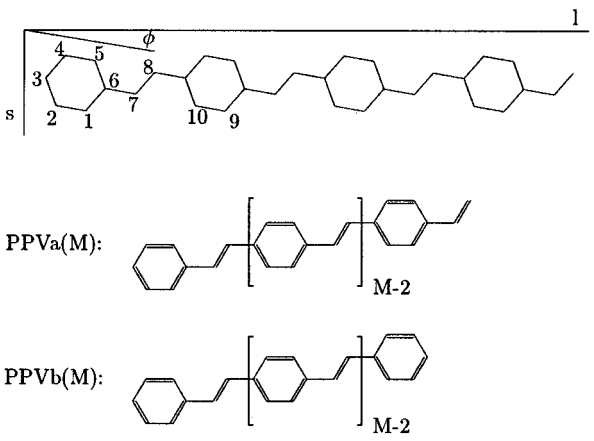

FIG. 1. Geometry and labeling of the monomeric unit of PPV oligomers. Bond angles are 120°, except $\alpha(\mathbf{r}_{6,7},\mathbf{r}_{7,8})=128°$, and distances are: $r_{1,2}=r_{2,3}=r_{3,4}=r_{4,5}=r_{5,6}=r_{6,1}=1.39$ Å, $r_{6,7}=1.44$ Å, $r_{7,8}=1.33$Å. PPVb is a symmetric oligomer obtained from PPVa by eliminating the terminating vinylene group.

is the Greens' function of the homogeneous problem.

The computation of the linear polarizability α, which relates the expectation value of the polarization to the driving field is carried out in two steps. First the TDHF equations are

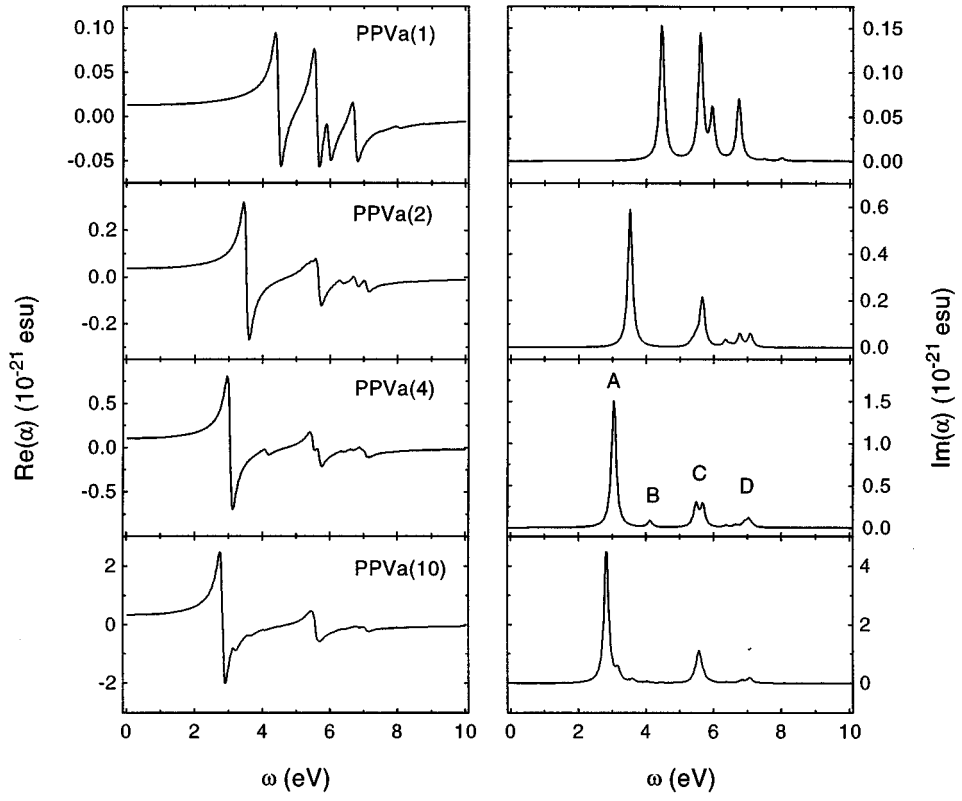

FIG. 2. Real (left) and imaginary (right) part of the linear polarizability α for PPVa(M), with $M=1,2,4,10$. A,B,C,D indicate four distinct bands which develop for large oligomers.

solved for the source term A_{nm}. This yields the induced charges $\delta\rho_{nn}$ to first order in the driving field. In the second step we compute the polarization using Eq. (7) and obtain

$$\mathbf{P}(\mathbf{r},\omega)=\int d\mathbf{r}'\,\vec{\vec{\alpha}}(\mathbf{r},\mathbf{r}';\omega)\cdot\mathbf{E}(\mathbf{r}',\omega), \tag{24}$$

where the nonlocal polarizability tensor is given by

$$\vec{\vec{\alpha}}(\mathbf{r},\mathbf{r}';\omega)=\sum_{nm}\tilde{\alpha}_{nm}(\omega)\vec{\mathscr{P}}_n(\mathbf{r})\vec{\mathscr{P}}_m(\mathbf{r}'). \tag{25}$$

Here $\vec{\mathscr{P}}_n(\mathbf{r})\vec{\mathscr{P}}_m(\mathbf{r}')$ denotes the tensorial product, which we write as a dyadic. The response functions $\tilde{\alpha}_{nm}$ defined in Eq. (22) are characteristic molecular quantities. They describe the effects of the field interaction V_m with the charge distribution on atom m on the charge at atom n. These key quantities for the computation of the optical polarizabilities will be investigated below. The local polarizabilities computed in Ref. 19 are obtained by applying a homogeneous field and imposing the dipole approximation. The total polarization of the molecule is then an induced dipole, which is related to the driving field by $\mathbf{P}(\omega)=\vec{\vec{\alpha}}(\omega)\mathbf{E}(\omega)$, and the total polarizability tensor $\vec{\vec{\alpha}}$ is given by

$$\vec{\vec{\alpha}}(\omega)=\sum_{nm}\tilde{\alpha}_{nm}(\omega)\mathbf{r}_n\mathbf{r}_m, \tag{26}$$

where we chose the reference point $\mathbf{R}=\mathbf{0}$. The diagonal tensor components $\alpha(\mathbf{n},\omega)=\mathbf{n}\cdot\vec{\vec{\alpha}}(\omega)\cdot\mathbf{n}$ can be written in Drude form

$$\alpha(\mathbf{n},\omega)=N\frac{e^2}{m^*}\sum_{\nu}\frac{f_\nu(\mathbf{n})}{(\omega+i\Gamma)^2-\Omega_\nu^2}, \tag{27}$$

where m^* is an effective mass, determined by the sum rule $\Sigma f_\nu=1$, and Γ is a damping constant, set to $\Gamma=0.08e\text{Å}^4/\text{V}^3=1.0376\cdot10^{-35}$ esu. Expressions for the oscillator strengths $f_\nu(\mathbf{e}_z)$ were given in Ref. 19.

III. LINEAR POLARIZABILITY OF PPV OLIGOMERS

We have applied the method outlined in Sec. II to two types of PPV oligomers, referred to as PPVa(M) and PPVb (M), where M denotes the number of repeat units (see Fig. 1). PPVa is obtained by a simple repetition of the monomeric unit,[30] and has $N=8\cdot M$ carbon atoms. This oligomer is not inversion symmetric. In the second molecule (PPVb) we removed the terminating vinylene group (sites $8\cdot M-1,8\cdot M$) resulting in centro symmetric oligomers with $N=8\cdot M-2$ carbon atoms.

The electromagnetic field is assumed to be a plane wave, polarized parallel to the molecular plane (Fig. 1). Its in-plane orientation is defined by its angle ϕ with respect to the long chain axis ($\hat{\mathbf{l}}$). Unless indicated otherwise we set $\phi=0$, and $\alpha(\omega)=\alpha(\hat{\mathbf{l}},\omega)$.

The frequency dependent linear polarizability α for PPVa is shown in Fig. 2 for different sizes ($M=1,2,4,10$). The spectra are dominated by very few bands, and the strongest absorption is always the lowest band A, whose frequency depends markedly on oligomer size. The position of the second intense absorption band C—centered around ≈5.5 eV—hardly depends on the chain length, only its shape becomes narrower and it seems to be dominated by a single line for longer oligomers. We further observe two weaker absorption features. For $M>2$, a small peak B occurs between the main absorption bands, which is red shifted with increasing oligomer size. And in the UV there is a peak centered around 7 eV, which hardly depends on oligomer size. The overall convergence pattern suggests that $M=10$ repeat units essentially represent an infinite polymer. For a more quantitative analysis we display the energy Ω_A of the lowest absorption A, its oscillator strength f_A, and the effective mass m^*, as a function of M in Fig. 3. f_A converges already at small oligomer sizes $M>5$, implying a linear size scaling of the polarizability, whereas Ω_A has a larger saturation length $M\gtrsim10$. Contrary to these quantities, characterizing the low-energy end of the spectrum, the effective mass is determined by the entire spectrum and still varies somewhat at the largest size studied ($M\approx10$).

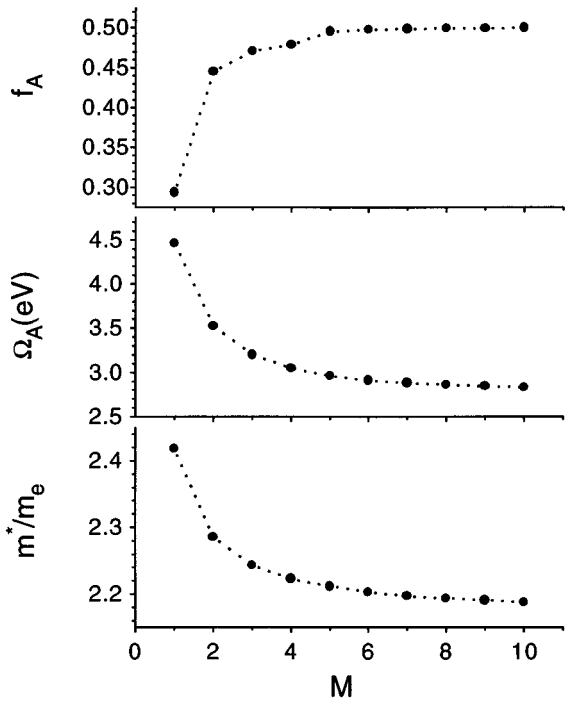

FIG. 3. Convergence with size of the oscillator strength f_A of the lowest absorption line, its frequency Ω_A (the optical gap), and the effective mass m^*. f_A converges most rapidly and at $M=5$ it essentially reaches its asymptotic value. Ω_A saturates at about $M=10$ where m^* still depends weakly on size.

Although we used optimized parameters for polyacetylene[19] without any adjustment to PPV we find the calculated absorption frequencies to be in good agreement with previous studies. The convergence of the energy gap is similar to the results of Wang *et al.*,[31] who used a Su-Schrieffer-Heeger (SSH)—type Hamiltonian (which does not include e-e correlations) in the investigation of vibrational properties of PPV. Their (neutral) band gap also converges for

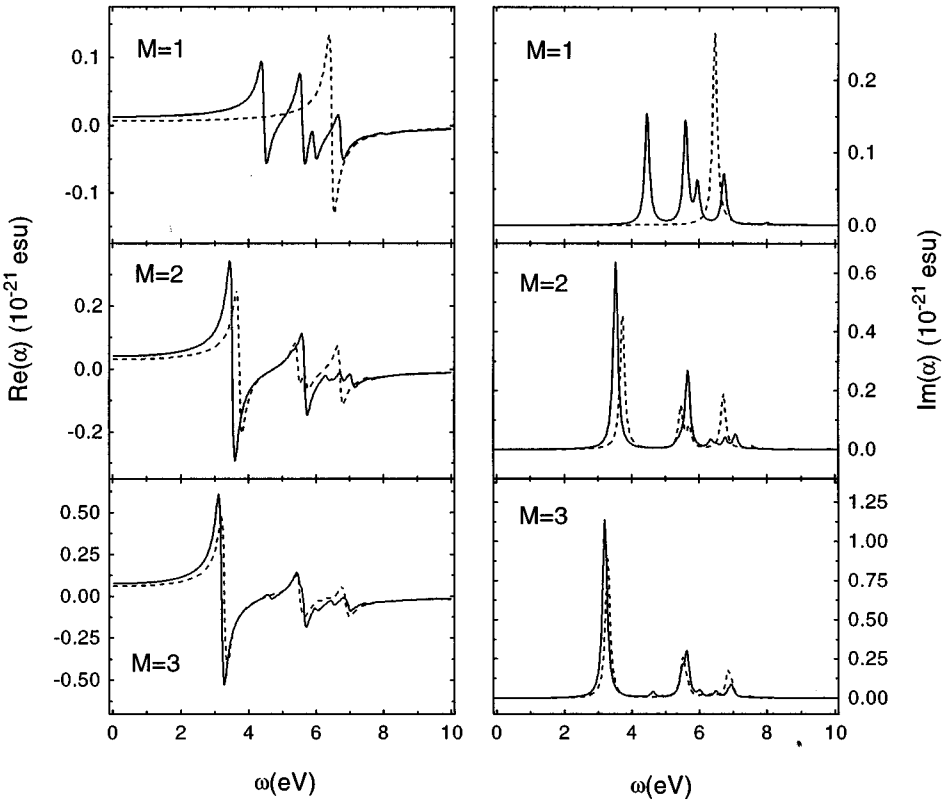

FIG. 4. Real (left) and imaginary (right) part of the linear polarizability α for PPVa(M) (solid) and PPVb(M) (dashed) for $M=1,2,3$ as indicated.

$M\approx 10$. This illustrates that it is possible to mimic the saturation length properly without including explicitly e-e correlations (these correlations are included implicitly by the SSH parametrization). Our energy gaps agree with those reported in Ref. 31 to within 13%. The lowest absorption frequency is in good agreement with infrared spectra of PPVb(3), up to PPVb(7).[5,6] For PPVb(3) the difference is less than 1%, and for larger oligomer sizes it increases, but stays below 10%. Note, that the lowest-energy transition in Fig. 5 of Refs. 5 and 6 is not the maximum of the peak, but the shoulder ($\approx 0.15-0.20$ eV below the maximum). This is due to disorder, affected by the preparation process of the oligomers and discussed in Refs. 1 and 3. Also the frequency of the intermediate peak B, which develops for $M>2$ in our model, is reproduced to within 3% for $M>4$. The error decreases with increasing size. We find for the frequency of the size-independent peak C a value, which is too large by 16%. This deviation cannot be explained by the neglect of other valence electrons from σ-bonds, as J. Cornil *et al.*[17] use a sum over state technique including all valence electrons, and find an even larger frequency for this peak.

In order to study the role of the terminating vinylene group we compare the linear absorption of PPVa and PPVb for the three oligomers $M=1,2,3$ in Fig. 4. The difference is most striking for $M=1$, where the symmetric benzene ring is characterized by a single absorption peak. The symmetry breaking by the vinylene group in the corresponding styrene results in four distinct peaks. For longer oligomers the dominant absorption is red shifted and the spectra show a richer structure. However, with increasing length the overall effect of the terminating vinylene group becomes less pronounced, and the absorption converges towards the same limit.

We next investigate the tensorial properties of $\vec{\vec{\alpha}}$ by comparing the absorption of PPVa(4) for two polarizations, parallel and perpendicular to the long oligomer axis. The most striking observation of Fig. 5 is a blue shift of the dominant absorption for perpendicular polarization. In this case band C, which depends only weakly on chain length, has the dominant absorption in terms of oscillator strength. Also, absorption peaks at higher frequencies are strongly enhanced. This is not surprising, considering the delocalized nature of the electrons. It takes little energy to displace them in the chain direction, whereas a perpendicular field cannot excite such longitudinal oscillations.

Following this observation, we computed the full angular dependence of the linear response function. Since $\tilde{\alpha}_{nm}$ is a symmetric tensor, the directions of minimum and maximum absorption (its principal axes) must be orthogonal. Therefore we plot only the angle of maximum absorbance as a function of frequency in Fig. 6. This figure also shows the angular dependence of the absorbance at six selected frequencies, marked as vertical lines in Fig. 5. These are periodic functions with periodicity π, and their minima (maxima) give the direction of minimum (maximum) absorbance.

Up to a frequency of ≈ 4 eV, the maximum absorbance occurs at $\phi\approx 173°$, i.e. almost parallel to the long axis. This

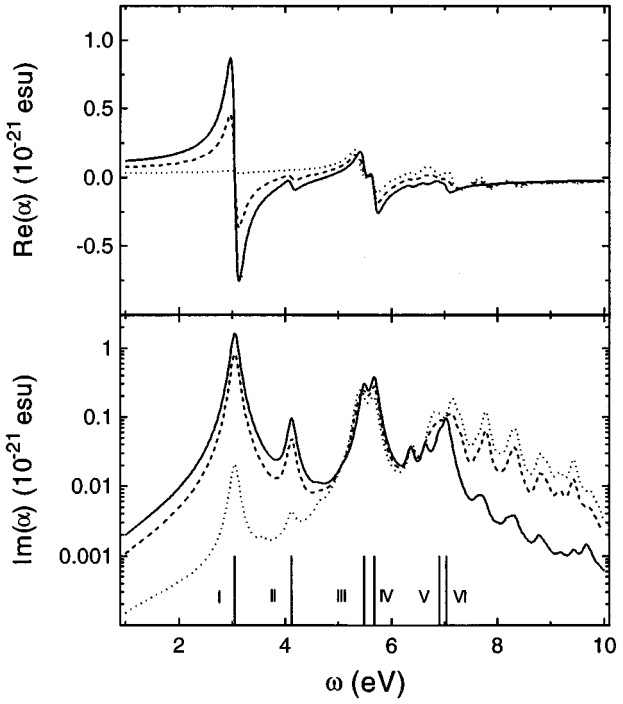

FIG. 5. Comparison of parallel ($\phi=0$, solid) and perpendicular ($\phi=90°$, dotted) polarizabilities of PPVa(4). Also shown are the orientational averaged polarizabilities (dashed lines, see text). The vertical lines, labeled I to VI, indicate the positions of the strongest six transitions.

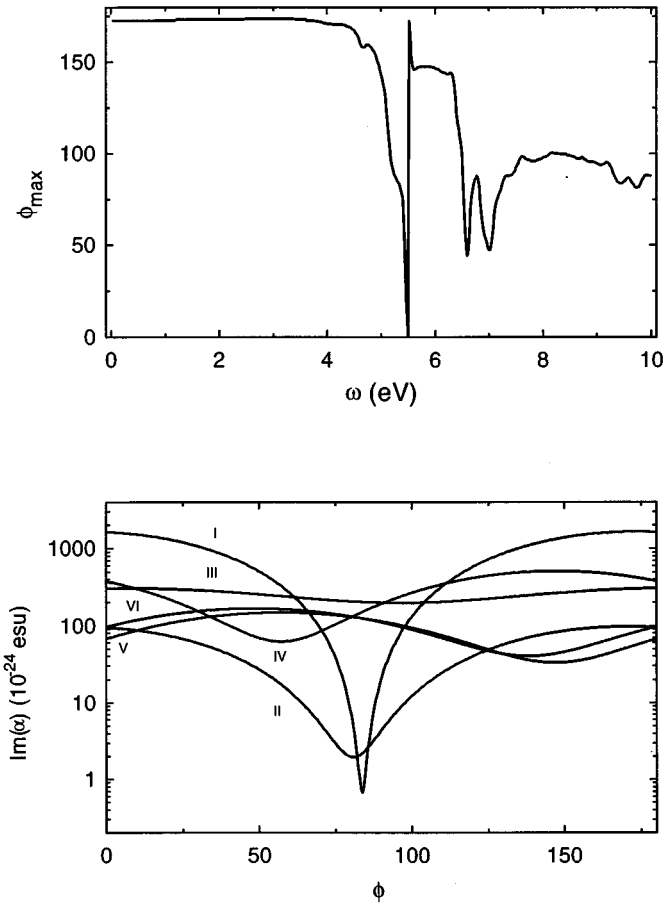

FIG. 6. Anisotropy of the linear polarizability of PPVa(4). The bottom graph shows the angular dependence of the absorption $\mathrm{Im}(\alpha)$ at the six selected frequencies shown in Fig. 5. Φ is given in degrees. The top graph shows the angle ϕ_{max} of maximum absorbance as a function of frequency. Angles are measured with respect to the long axis (see Fig. 1).

can be expected due to the high polarizability of electrons along the delocalized π-network. Therefore the absorbance of the 3.05 eV mode drastically decreases, as the angle approaches $\phi\approx 90°$. The same holds for the 4.12 eV mode. Both oscillators are associated with delocalized, longitudinal oscillations, and, therefore depend on oligomer size. As the third band C is approached, the angle of maximum absorbance reaches 90° and switches back to $\approx 180°$. The orientational independence of the 5.48 eV absorption further suggests that the corresponding excitation is localized within the phenylene groups. Oscillations perpendicular to the long axis also show up at frequencies >7.5 eV. In the frequency range between these extremes, several orientations of maximum absorbance occur, as shown in Fig. 7.

We conclude this section by presenting the nonlocal response function $\tilde{\alpha}_{nm}$ for PPVa(8) for selected frequencies in Fig. 8. We have computed all optical transitions and discuss only the eight strongest ones, whose oscillator strength is larger than 3% of f_A. The absorption spectrum of PPVa(8) is almost identical to that of PPVa(10) shown in Fig. 2, so that we did not repeat it here. At $\Omega_A=2.86$ eV, significant correlations between atoms up to six units apart (i.e. $|n-m|<6\cdot 8$) show up. This reflects the onset of saturation and suggests an effective conjugation length of 6 repeat units or 48 carbon atoms. However, this is only a rough, qualitative estimate influenced by finite size effects, which lies markedly below the value established in Fig. 3. The levelling-off at the ends of the oligomer parallel the same behavior for HOMO and LUMO (see next section). The maxima of the polarizability occur between carbon atoms on the vinylene groups, so that the bridge states between the phenylene rings are of crucial importance for the low-energy optical dynamics in PPV. This finding is at variance with the

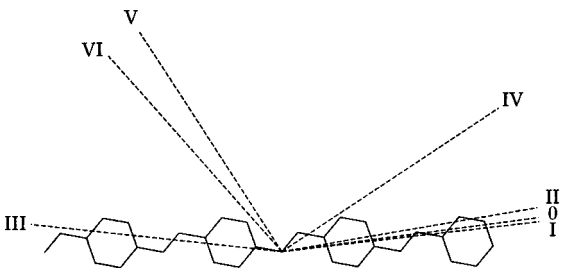

FIG. 7. Directions of maximum absorbance of PPVa(4) for the six peaks shown in Fig. 5 as well as for the zero frequency (0). The angles for the various peaks are: 172.8°(0), 173.7°(I), 170.6°(II), 6.30°(III), 147.2°(IV), 56.77°(V), 48.1°(VI).

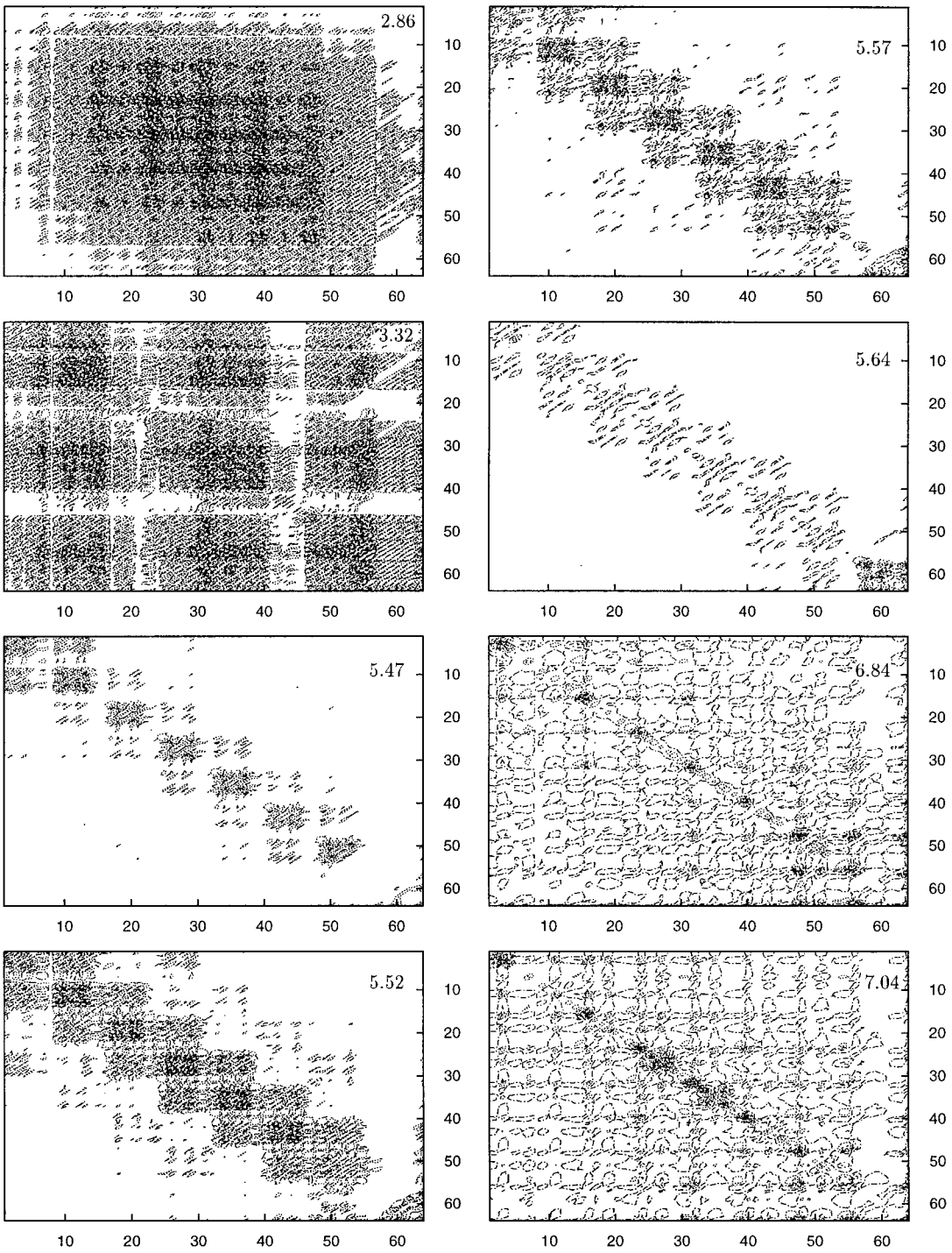

FIG. 8. Contour plot of the nonlocal linear polarizability $\mathrm{Im}(\tilde{\alpha}_{nm})$ of PPVa(8) calculated at eight frequencies, corresponding to the strongest peaks in the linear absorption. We used five contour lines, chosen automatically by the plotting software (gnuplot), the lowest one being $\approx 10\%$ of the largest one (in magnitude). The corresponding frequencies (in eV) are indicated in the upper right corner of each panel. The oscillator strengths at these frequencies are 0.500, 0.044, 0.055, 0.064, 0.061, 0.105, 0.016, 0.045.

assumption of Rice and Gartstein,[18] who propose a system of coupled benzene rings for the interpretation of the optical response of PPV.

As mentioned above, the absorption at 3.32 eV corresponds to the small peak B between the two main absorption maxima, which eventually turns into a shoulder of the lowest-energy peak A, as the oligomer-size increases. A glance at its polarizability α_{nm} shows that the third and sixth units are almost inactive at this frequency. Generally two neighboring units are strongly coupled, and these units in turn couple only to other units, which are $2j$ units away, where j is an integer. Obviously the estimate of the coher-

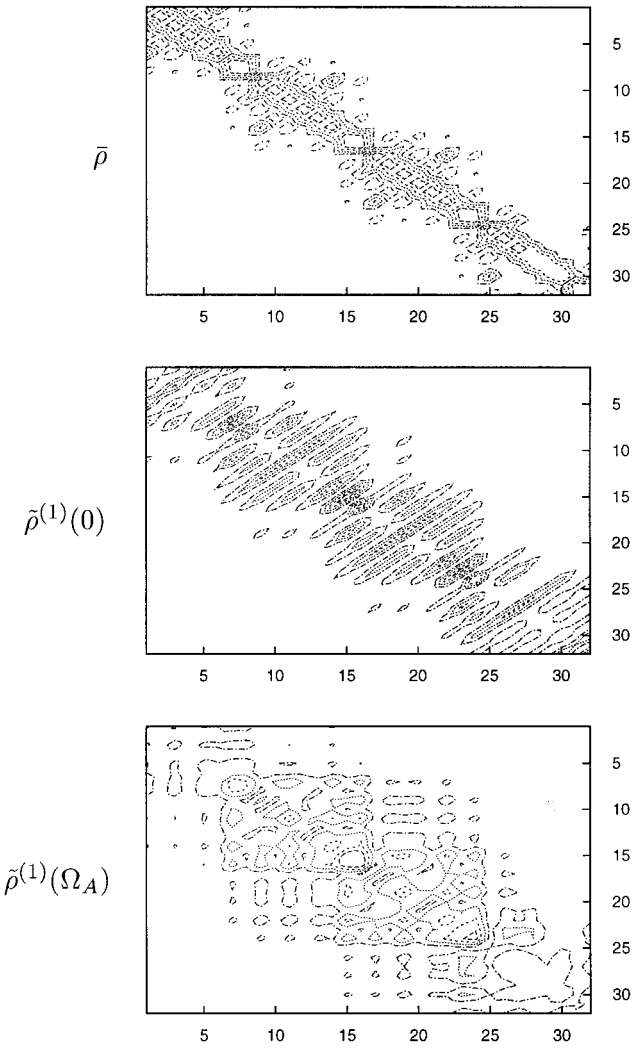

FIG. 9. The top graph shows the reduced one-electron ground state density matrix $\overline{\rho_{nm}}$ of PPVa(4) in the site representation. Diagonal elements $\overline{\rho_{nn}}=0.5$ denote the electron charge. Off-diagonal matrix elements ρ_{nm} are a measure for the strength of the chemical bond between sites n and m. The other two panels show the density matrix to first order in the field at $\omega=0$ (middle panel) and at the lowest absorption frequency $\omega=\Omega_A$ (bottom panel). Note the significant electronic coherence (off diagonal elements) of $\delta\tilde{\rho}^{(1)}$ compared to $\overline{\rho}$.

ence size at this frequency is beyond 8 repeat units (64 sites), which is in accord with the marked size dependence of this absorption peak.

The next four transitions contributing to the second largest absorption peak C have very close energies (5.47,5.52,5.57,5.64 eV). Consequently, the polarizabilities have a very similar structure, characterized by large susceptibilities between atoms on neighboring units, i.e. if $|n-m|\leqslant 2\cdot 8$. Contrary to the lowest transition frequency, the largest polarizability for these four frequencies comes from atoms on the phenylene groups. From this graph the apparent conjugation length is 3, which compares well with the size dependence of the corresponding peak B in Fig. 2. For the last two transitions around (7 eV) the largest $\tilde{\alpha}_{nm}$ are the diagonal elements. With the exception of the outer atom in the vinylene group, the last repeat unit does not make a significant contribution.

IV. REAL SPACE ELECTRONIC OSCILLATOR ANALYSIS OF THE OPTICAL RESPONSE

In addition to providing a convenient computational scheme, the density matrix also allows a real space analysis of the spectra by relating them directly to the motions of electrons and holes, as well as to the dynamics of electronic coherences.[19] This is very different from the conventional chemical analysis in terms of eigenstates, and has many advantages. In this section we examine the density matrix and the electronic oscillator picture for PPV oligomers.

The reduced ground state one-electron density matrix $\overline{\rho_{nm}}$ for PPVa(4) is shown in Fig. 9. This graph illustrates the chemical bonding structure. Since we are not treating donor-acceptor substitutions, $\overline{\rho_{nn}}=0.5$ on all carbon atoms and the net charges $q_n=e(1-2\rho_{nn})$ vanish at all sites. Also shown are the off-resonant density matrix $\tilde{\rho}^{(1)}_{nm}(\omega=0)$ and the density matrix at the lowest absorption frequency $\tilde{\rho}^{(1)}_{nm}(\Omega_A)$. Both are delocalized over the entire molecule and show strong coherences between different repeat units. The block structure at Ω_A reflects the large extent of delocalization. It levels off at the oligomer ends because of finite size effects, and does not indicate a coherence length. The charges $\tilde{\rho}^{(1)}_{nn}(\Omega_A)$ indicate a polarization along the long axis **l**. The two carbon atoms of the vinylene groups carry charges of opposite sign and roughly the same magnitude. A similar charge separation in the direction of the long axis occurs within the phenylene rings. Atoms $2+8j$, $3+8j$, $4+8j$ have an opposite sign compared to those on sites $1+8j$, $5+8j$, $6+8j$, where $j=1,2,\ldots$.

A coupled electronic oscillator representation (CEO) for the linear and nonlinear response of conjugated molecules was developed in Refs. 19 and 25. The equations of motion were solved in the HFMO representation, yielding a set of coupled oscillators $\hat{Q}^{\nu}$, $\nu=1,\ldots,N^4/4$, which determines the linear and nonlinear response. For the current analysis we have computed these oscillators in the site representation $(Q^{\nu}_{nm}=\langle n|\hat{Q}^{\nu}|m\rangle)$ as well as in the HFMO representation $(Q^{\nu}_{\alpha\beta}=\langle\alpha|\hat{Q}^{\nu}|\beta\rangle)$. Here $|\alpha\rangle, \alpha=1,\ldots,N$ denote the HFMOs, numbered with increasing energy, so that the first $N/2$ are the occupied (particle), and the upper $N/2$ the unoc-

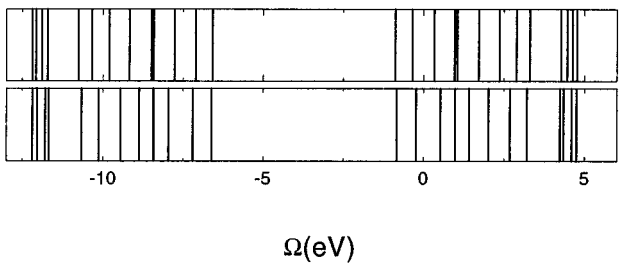

FIG. 10. Hartree Fock energies for PPVa(4) (top), and PPVb(4) (bottom). The states at the band edges are hardly affected by the terminating vinylene group. The HOMO for PPVb is red shifted by 34 meV, and the LUMO is blue shifted by 34 meV compared to PPVa.

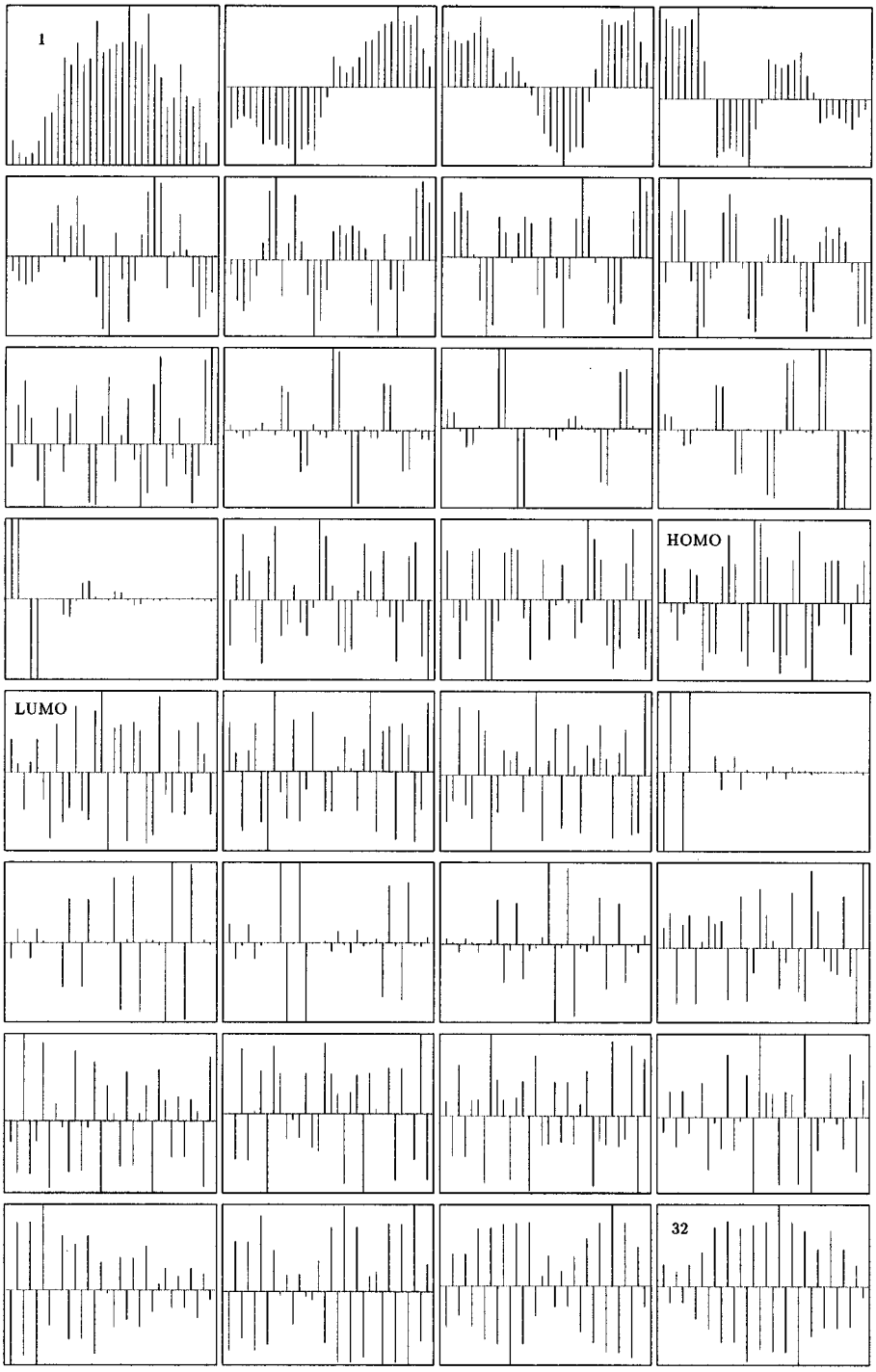

FIG. 11. HF molecular orbitals for PPVa(4), numbered with increasing energy from left to right, and from top to bottom.

cupied (hole) orbitals. Their site representation $c_{n\alpha}=\langle n|\alpha\rangle$ is depicted in Fig. 11 for PPVa(4). The HFMOs of PPVb(4) (not shown here) look quite similar, and the following statements hold for both types of oligomers. The corresponding HF energies are displayed in Fig. 10. HOMO (H) and LUMO (L) are delocalized states, which are not affected appreciably by the terminating vinylene group, as their energies differ only by 35 meV (0.5%). States in the interior of the valence band ($H-i, i=1,2,\ldots$) are generally delocalized over the entire molecule, with the exception of one state (H-3), which is localized. In case of the asymmetric PPVa-molecules this state is localized at the phenyl-end. For the symmetric molecules PPVb it is localized at both ends. This state belongs to an interesting group of states (H-3,H-4,H-5,H-6) having negligible amplitudes on the vinylene group. Another interesting feature of the HF states is that the only difference between $H-i$ and $L+i$ is that every other com-

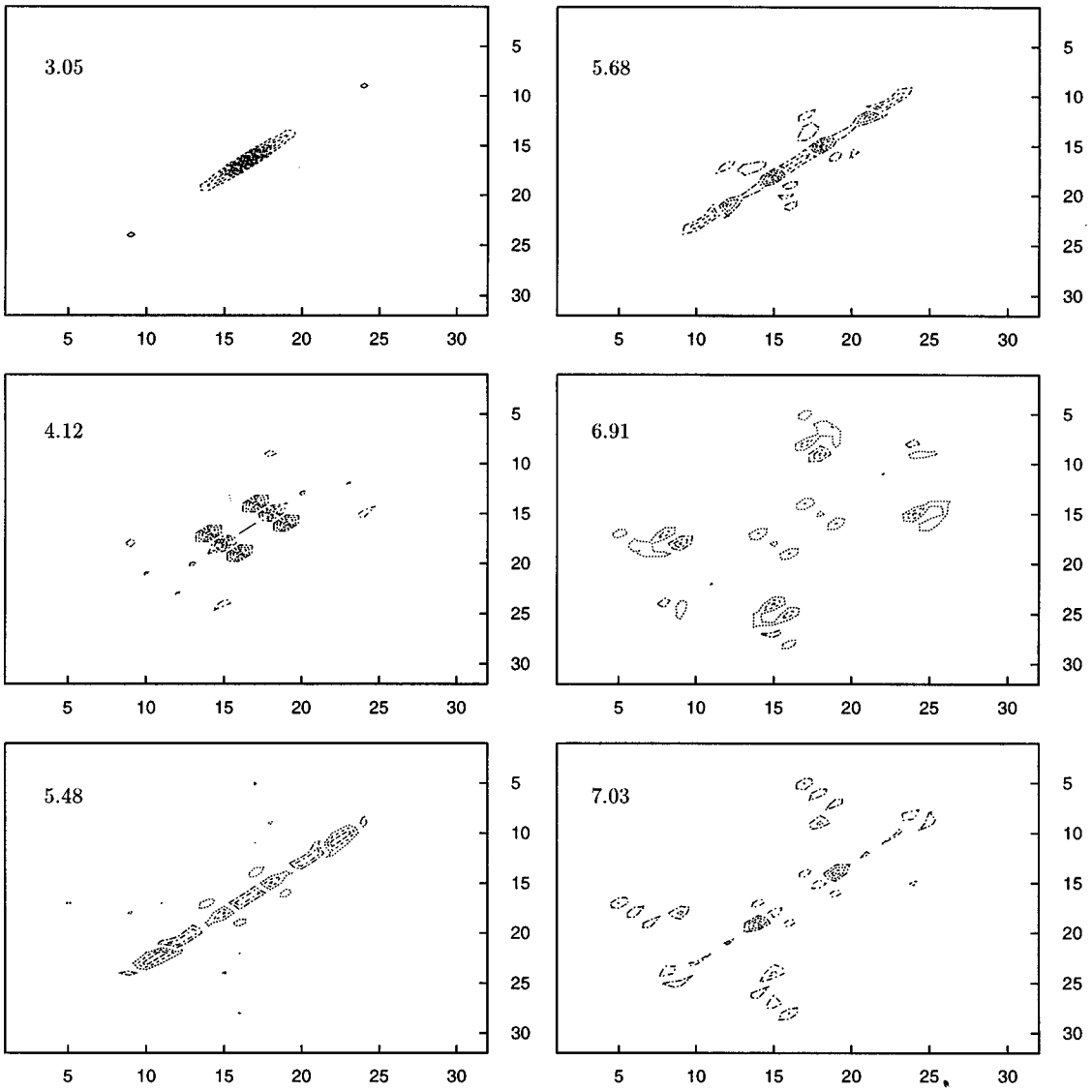

FIG. 12. Contour plot of the six dominant e-h oscillators Q_ν in the HFMO representation for PPVa(4). The oscillator frequencies (in eV) are indicated in each panel.

ponent differs in sign. This property can be shown analytically and is known as the pairing theorem.[32]

In order to investigate the physical origin of the different absorption features, we computed the coordinates Q^ν of the six most important oscillators with an oscillator strength exceeding 5% of the strongest oscillator. Since the arguments presented below hold for both types of molecules, we present this analysis only for PPVa(4).

By depicting the oscillators in the HFMO representation (Fig. 12), one clearly sees which HFMOs are involved at a given absorption line. The lowest peak always corresponds to the HOMO-LUMO transition as can be seen in Fig. 12, where the dominant coherence occurs between the levels $H:=N/2=16$ and $L:=N/2+1=17$. Secondary coherences between $H-i$ and $L+i$, $i=1,2,3$ are also present and carry 45%,26%,15% of the amplitude of the H-L transition for $i=1,2,3$. As can be seen from Fig. 11, all relevant HF states are delocalized.

The second peak B at 4.12 eV emerges for $M>2$ and is red-shifted with increasing chain length. For $M=10$ it turns into a shoulder of the main peak (see Fig. 2). This oscillator is characterized by three major coherences between $H-i$ and $L+3-i$, $i=0,1,2$ with the same magnitude, and the relevant states are again delocalized. Secondary coherences include an H-L transition and have amplitudes smaller than 30% of the main ones.

The absorption feature around 5.5 eV does depend only weakly on chain length, and comes from two oscillators, whose features are quite similar. The major coherences are between $H-i$ and $H+i$, $i=0,\ldots,5$, the dominant one being $i=5$. They fall into two categories. $i=0,1,2$ are transitions between delocalized states. These transitions depend strongly on the size (M). $i=3,4,5$ corresponds to the states mentioned above, which have no amplitudes on the vinylene group, and $i=3$ is a localized state. Matrix elements of an operator $\mathbf{O}$ between such states are consequently given by a

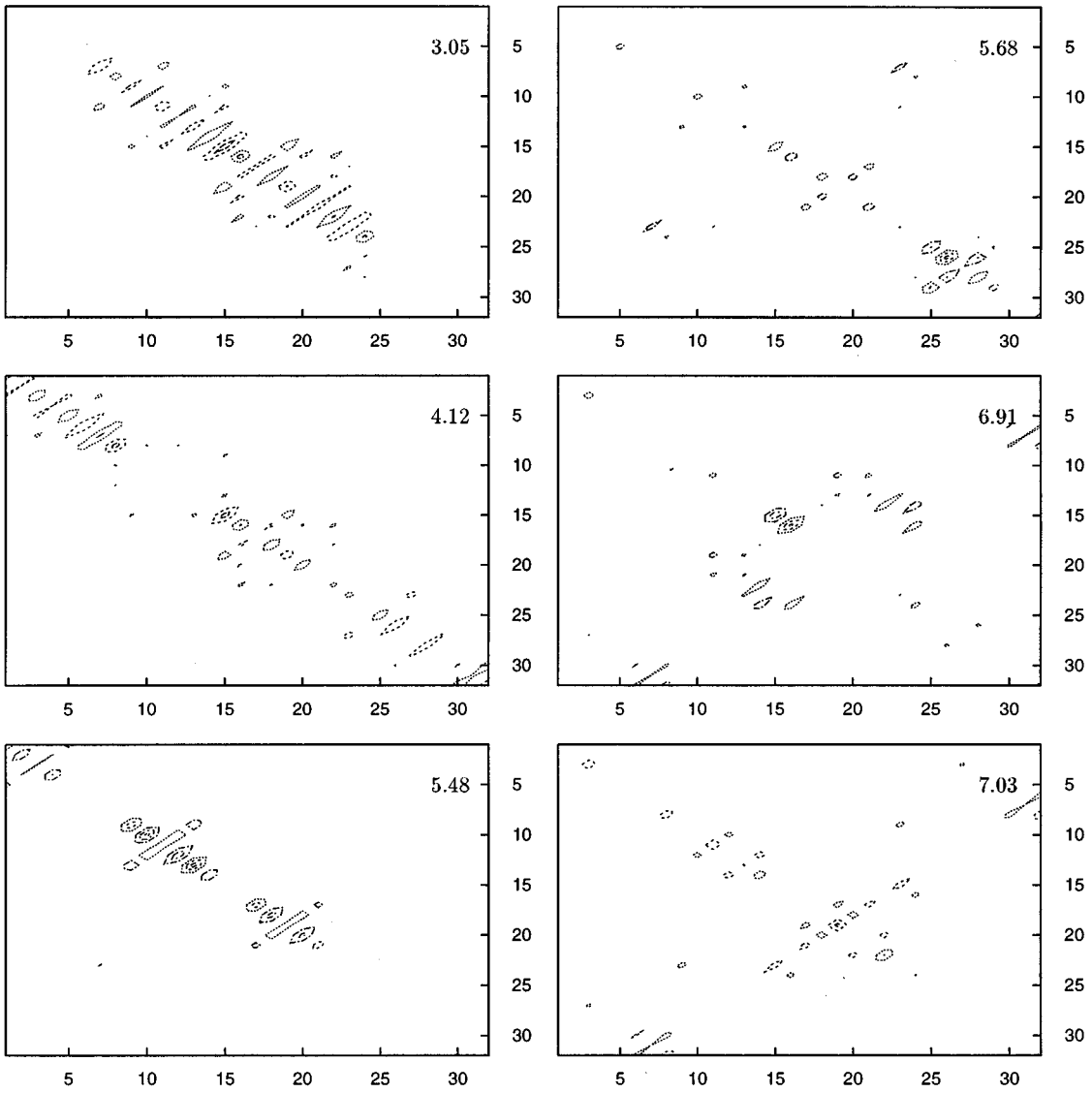

FIG. 13. Contour plot of the six dominant e-h oscillators Q_ν in the site representation for PPVa(4). The oscillator frequencies (in eV) are indicated in each panel.

sum of contributions from the phenylene groups (O_{p_j,p_j}) and couplings between them ($O_{p_i,p_j}, i \neq j$). Since the main cause of delocalization in our PPP Hamiltonian comes from nearest neighbor charge exchange, the coupling between different phenylene groups is negligible, and the matrix element can be written as a sum $\Sigma_j O_{p_j,p_j}$ over uncoupled phenylene groups. Therefore the peak associated with these two oscillators should depend only weakly on chain length. There are also minor coherences, such as $(H-5,L+4)$, $(H-4,L+5)$, $(H-2,L)$, $(H,L+2)$.

The absorption at about 7 eV is connected with the last two oscillators, which have a fundamentally different structure. Coherences $(H-i,L+i)$ only play a minor role, and other coherences dominate the oscillator. They are given by $H-i,L+j$. Each coherence has a counterpart $H-j,L+i$ with the same magnitude, which is a consequence of the electron-hole symmetry. The dominant ones are given by $(H-1,L+7)$, $(H,L+8)$, $(H,L+2)$. All states involved are delocalized.

Finally, a look at Q^ν in the site representation (Fig. 13) shows that the lowest-energy oscillator Q^A is delocalized over the molecule and has considerable coherences between different repeat units. This is to be expected in view of the strong size dependence of peak A.

V. SUMMARY

We have investigated the anisotropic, linear polarizability of poly(p-phenylene vinylene) (PPV) oligomers using the Pariser-Parr-Pople (PPP) Hamiltonian. By solving the time dependent Hartree Fock (TDHF) equations to first order in the electric field, we obtained a nonlocal response function $\tilde{\alpha}_{nm}(\omega)$, describing the effects of a field interaction at site m on the charge at site n [Eq. (22)]. It is then possible to

calculate the complete nonlocal optical polarizabilities $\vec{\alpha}(\mathbf{r},\mathbf{r}';\omega)$ using Eq. (25). It is not necessary to invoke the dipole approximation, as the full polarization densities $\vec{\mathcal{P}}(\mathbf{r})$ can be calculated. However, in the computation of the total polarizabilities of oligomers we applied a homogeneous field and invoked the dipole approximation.

By calculating the optical absorption of oligomers with up to 10 repeat units, we found that the oscillator strength of the lowest absorption line begins to scale linearly with size at $M=5$ repeat units. The optical gap converges at a larger size of 10 units. This is in good agreement with other experimental and theoretical results.[5,6,31] Also, the calculated absorption spectrum compares well with experiment.[5,6] We used the same parameter set used to describe polyenes successfully, and our method provides a good description of the photophysics of both systems.

We further calculated the orientational dependence of the resonant polarizability via Eq. (26). We found that absorption with polarization perpendicular to the long chain axis predominantly occurs at higher frequencies. The lowest peak A (Fig. 2) does not carry the largest oscillator strength, it is the band C around 5.5 eV which dominates the absorption. Upon orientational averaging, which corresponds to an unoriented sample, the qualitative behavior is changed only slightly (see Fig. 5). The magnitude of the averaged first absorption has decreased, the second intense band remains virtually unchanged, and the averaged absorption for higher bands is increased. Thus the basic conclusions of an analysis with parallel polarization remain unchanged when applied to an unoriented sample. The analysis of the orientation dependence yielded the principal axis of $\vec{\alpha}(\omega)$, which we computed for the six most dominant peaks in the spectrum(see Fig. 7). The lowest two absorption bands A and B could be associated with longitudinal charge oscillations, and band D beginning at 7 eV with transverse oscillations. The middle band C around 5.5 eV has one mode with transverse oscillations, and the modes between 5.5 eV and 7 eV exhibit a more complicated dynamics.

We next studied the nonlocal response function $\tilde{\alpha}_{nm}(\omega)$ for PPVa(8) in order to gain a better insight on electronic dynamics. Plotting these quantities at selected frequencies in the site representation shows correlations between subsections of the molecule. At the lowest electronic transition, dominant correlations occur between units, as far apart as 4 or 5 repeat units. At this frequency electrons are completely delocalized over the interior of the molecule, which reflects the HOMO and LUMO wave functions. Moreover, the nonlocal polarizability reveals that the lowest absorption can be best excited at vinylene groups, and the corresponding polarization stems also from vinylene groups. This finding suggest that a model for the lowest-energy absorption has to contain specific details of the bridges connecting the phenylene rings. For the second peak B (centered around 3.32 eV for $M=4$), which is also characterized by transitions between delocalized HFMO states such correlations occur even over 6 units, the main ones occurring between units 3 repeat units apart. The absorption band C, which depends only weakly on frequency is characterized by correlations between units next to each other. A field interaction at one unit predominantly affects neighboring units, so that the total response is the sum of such (similar) contributions; this results in a rapid convergence with size.

We finally analyzed our results in terms of the coupled electronic oscillator (CEO) representation. It was shown earlier,[19,25] that the TDHF equations can be mapped onto a set of coupled harmonic oscillators Q^{ν}, which fully describes the system under investigation. For polyenes the linear absorption is governed by one oscillator. Our calculation for PPV showed that up to 8 oscillators are necessary for describing the resonant linear response of the studied oligomers. By expanding the relevant eigenmodes in the Hartree Fock Molecular Orbital (HFMO) representation we could study the underlying transitions between the HFMOs. The lowest oscillator carries 50% of the oscillator strength and is dominated by HOMO-LUMO transitions. The calculated HFMOs show clearly, that HOMO and LUMO are delocalized over the entire molecule. In the same manner we investigated the other dominant oscillators and identified the transitions responsible for a particular absorption. The most notable result is the structure of the states responsible for the absorption band C. The dominant amplitudes of Q^{ν} come from transitions between states, which are localized on the phenylene rings. Another strong transition involves the state, which is localized at the phenyl-end of PPVa(M), or at both ends of PPVb(M). This explains the weak size dependence of the corresponding absorption band C. The present approach can be extended to the computation of nonlinear response functions, and to the inclusion of intermolecular interactions and local field effects.

ACKNOWLEDGMENTS

We would like to thank Guanhua Chen for many fruitful discussions. This work was made possible by an E. Schrödinger Stipendium (grant J-01023-PHY) from the Fonds zur Förderung der Wissenschaftlichen Forschung, Austria, which one of us (Th.W.) gratefully acknowledges. The support of the Air Force Office of Scientific Research and the National Science Foundation is gratefully acknowledged. We are also thankful for CPU time on a C90 granted by Air Force major shared resource centers (MSRC).

[1] T.W. Hagler, K. Pakbaz, K.F. Voss, and A.J. Heeger, Phys. Rev. B **44**, 8652 (1991);
[2] P.L. Burn *et al.*, Springer Series in Solid-State Sciences **107**, 107 (1992).
[3] D.A. Halliday *et al.*, Synthetic Metals **55-57**, 954 (1993); K. Pichler *et al. ibid.* **55-57**, 230 (1993).
[4] D.D.C. Bradly, R.H. Friend, H. Lindenberger, and S. Roth, Polymer **27**, 1709 (1986).
[5] A. Sakamoto,Y. Furukawa, and M. Tasumi, J. Chem. Phys. **96**, 1490 (1992); **96**, 3870 (1992).
[6] B. Tian, G. Zerbi, R. Schenk, K. Müllen, J. Chem. Phys. **95**, 3191 (1991); B. Tian, G. Zerbi, and K. Müllen, *ibid.* **95**, 3198 (1991).
[7] N.F. Colaneri *et al.*, Phys. Rev. B **42**, 11670 (1990).
[8] U. Rauscher, H. Bässler, D.D.C. Bradley, and M. Hennecke, Phys. Rev. B **42**, 9830 (1990).

[9] J. Swiatkiewicz, O.N. Prasad, and F.E. Karasz, J. Appl. Phys. **74**, 525 (1993).
[10] T.W. Hagler, K. Pakbaz, and A. J. Heeger, Phys. Rev. B **49**, 10 968 (1994); *ibid.* **51**, 14 199 (1995).
[11] J.W.P. Hsu *et al.*, Phys. Rev. B **49**, 712 (1994); M. Yan *et al.*, Phys. Rev. Lett. **72**, 1104 (1994); M. Yan *et al.*, Phys. Rev. B **49**, 9419 (1994).
[12] R. Kersting *et al.*, Phys. Rev. Lett. **70**, 3820, (1993); B. Mollay *et al.*, Phys. Rev. B **50**, 10769 (1994).
[13] J.L. Bredas, R.R. Chance, R.H. Baughman, and R. Silbey, J. Chem. Phys. **76**, 3673 (1982).
[14] C.B. Duke and W.K. Ford, Int. J. Quant. Chem. Symp. **17**, 597 (1983).
[15] P. Gomes da Costa *et al.*, Synthetic Metals **55–57**, 4320 (1993).
[16] J. Obrzut and F.E. Karasz, J. Chem. Phys. **87**, 2349 (1987).
[17] J. Cornil, D. Beljonne, R.H. Friend, J.L. Bredas, Chem. Phys. Lett. **223**, 82 (1994).
[18] M.J. Rice and Yu.N. Gartstein, Phys. Rev. Lett. **73**, 2504 (1994).
[19] A. Takashashi and S. Mukamel, J. Chem. Phys. **100**, 2366 (1994); S. Mukamel, A. Takashashi, H.X. Wang, and Guanhua Chen, Science **265**, 250 (1994).
[20] K.L.C. Hunt and Y.Q. Liang, J. Chem. Phys. **95**, 2549 (1991); K.L.C. Hunt, Y.Q. Liang, R. Nimalakirthi, and R.A. Harris, *ibid*. **91**, 5251 (1989); P.H. Liu and K.L.C. Hunt, *ibid*. **100**, 2800 (1994); Ying Q. Liang and K.L. C. Hunt, *ibid*. **98**, 4626 (1993).
[21] H. Ishihara and K. Cho, Phys. Rev. B **48**, 7960 (1993).
[22] J.K. Jenkins and S. Mukamel, J. Chem. Phys. **98**, 7046 (1993).
[23] V. Chernyak and S. Mukamel, Phys. Rev. B **48**, 2470 (1993).
[24] M. Hartmann, V. Chernyak, and S. Mukamel, Phys. Rev. B **52**, 2528 (1995).
[25] G. Chen and S. Mukamel, J. Am. Chem. Soc. **117**, 4945 (1994); G. Chen and S. Mukamel, Chem. Phys. Lett. **240**, 296 (1995).
[26] H. Fukutome, J. Mol. Struct. (Theochem) **188**, 337 (1989), and references therein.
[27] D.P. Craig and T. Thirunamachandran, *Molecular Quantum Electrodynamics* (Academic, 1984); E. A. Power, *Introductory Quantum Electrodynamics* (Academic, New York, 1984).
[28] A. Szabo and N.S. Ostlund, *Modern Quantum Chemistry* (McGraw-Hill, New York, 1982).
[29] R. McWeeny, Rev. Mod. Phys. **32**, 335 (1960); G. Diercksen and R. McWeeny, J. Chem. Phys. **44**, 3554 (1966); R. McWeeny, Chem. Phys. Lett. **1**, 567 (1968).
[30] Thierry Granier *et al.*, J. Polym. Sci. **24**, 2793 (1986).
[31] W.Z. Wang, A. Saxena, and A.R. Bishop, Phys. Rev. B **50**, 6068 (1994).
[32] M.J.S. Dewar, *Molecular Orbital Theory of Organic Chemistry* (McGraw-Hill, New York,1969); H. Bock and E. Heilbronner, *The HMO Model and its Applications* (Wiley, New York, 1976).